# Response to a Steady Poleward Outflow. Part I: The Linear, Quasigeostrophic Problem

THEODORE S. DURLAND

*College of Oceanic and Atmospheric Sciences, Oregon State University, Corvallis, Oregon*

JOSEPH PEDLOSKY AND MICHAEL A. SPALL

*Woods Hole Oceanographic Institution, Woods Hole, Massachusetts*

## ABSTRACT

The response of a zonal channel to a uniform, switched-on but subsequently steady poleward outflow is presented. An eastward coastal current with a Kelvin wave's cross-shore structure is found to be generated instantly upon initiation of the outflow. The current is essentially in geostrophic balance everywhere except for the vicinity of the outflow channel mouth, where the streamlines must cross planetary vorticity contours to feed the current. The adjustment of this region generates a plume that propagates westward at Rossby wave speeds. The cross-shore structure of the plume varies with longitude, and at any given longitude it evolves with time. The authors show that the plume evolution can be understood both conceptually and quantitatively as the westward propagation of the Kelvin current's meridional spectrum, with each spectral element propagating at its own Rossby wave group velocity.

## 1. Introduction

This paper presents the linear quasigeostrophic (QG) response to a switched-on, steady outflow from a poleward-facing channel mouth (see Fig. 1). It is a companion paper for Durland et al. (2008, hereafter DSP), where the results derived herein are used as a foundation for understanding the equivalent problem in the framework of the nonlinear shallow-water equations (SWE) on the $\beta$ plane.

The physical motivation for the overall investigation lies in the remarkable coincidence between features of the SWE solutions and observations of eddy variability in the eastern Indian Ocean, just poleward of Lombok Strait. The observed eddies have variously been attributed to baroclinic instability of the South Equatorial Current (SEC) (Feng and Wijffels 2002), barotropic instability of the SEC (Yu and Potemra 2006), and eddy shedding by the branch of the Indonesian Throughflow (ITF) entering the Indian Ocean as a predominantly zonal flow through Timor Passage (Nof et al. 2002). DSP demonstrate that a highly idealized $1\frac{1}{2}$-layer model of

the poleward-flowing branch of the ITF exiting Lombok Strait produces eddy variability with temporal and spatial patterns quite similar to those observed, indicating the presence of a contributory mechanism that has not previously been considered. A more complete description of relevant observations, prior modeling work, and the nonlinear model results can be found in DSP.

The linear QG model considered in this paper does not support eddy generation, but it clearly elucidates the origins of two important dynamical features that are also found in the nonlinear SWE solutions: an eastward-propagating coastal Kelvin wave that sets up rapidly upon initiation of the outflow and a plume that propagates westward from the outflow at the long Rossby wave speed. In particular, an approximation to the QG solution provides a conceptual and quantitative description of the plume evolution, and DSP use this description to help explain the nonlinear model's behavior west of the outflow mouth where the eddies appear.

The term *poleward* describes a meridional flow directed away from the equator, whether in the Northern or Southern Hemisphere. Solutions will be presented from a Northern Hemisphere (NH) perspective (as in Fig. 1), but we note that the Southern Hemisphere response to a poleward outflow is merely a reflection across the equator of the NH results, which we will display.

*Corresponding author address:* Theodore S. Durland, College of Oceanic and Atmospheric Sciences, Oregon State University, Corvallis, OR 97331.
E-mail: tdurland@whoi.edu

A northward outflow in the Northern Hemisphere problem becomes a southward outflow in the equivalent Southern Hemisphere problem, and westward (eastward) propagation in the Northern Hemisphere problem remains westward (eastward) propagation in the Southern Hemisphere scenario. The mathematical model is presented in section 2, solutions in section 3, and a summary of the results in section 4.

## 2. Model

The linear, inviscid, nondimensional quasigeostrophic vorticity equation for shallow-water theory is (Pedlosky 1987)

$$(\nabla^2 - 1)\partial_t \psi + \beta \, \partial_x \psi = 0, \tag{1}$$

where $\psi$ is the streamfunction ($\partial_x \psi = v, \partial_y \psi = -u$), $x$ and $y$ are the eastward and northward Cartesian coordinates, and $u$ and $v$ are the zonal and meridional components of velocity. The normalization is $(x^*, y^*) = (x, y)L_d$, $t^* = t f_0^{-1}$, and $(u^*, v^*) = (u, v)L_d f_0$, where asterisks denote dimensional variables; $f_0$ is the Coriolis parameter and $L_d$ the deformation radius at the outflow latitude; the origin of coordinates is chosen at the center of the outflow channel mouth (Fig. 1). The nondimensional $\beta$ is equal to $\beta_0 L_d/f_0$, where $\beta_0$ is the meridional derivative of the Coriolis parameter at the outflow latitude.

The initial condition is

$$\psi(x, y, t < 0) = 0, \tag{2}$$

and we impose an outflow that is uniform across the channel mouth, switched on at $t = 0$, and steady thereafter. Our interest lies in the response of a semi-infinite basin, but to avoid the necessity of estimating two transform-inversion integrals, we formulate the problem in a zonal channel ($0 < y < L$). Once the discrete meridional modes are determined, they are summed numerically to convergence. In each solution presented, the channel width is chosen so that the boundary at $y = L$ does not significantly affect the solution during the integration time.

With the given normalization, the nondimensional outflow velocity is equal to the deformation-radius Rossby number ($Ro = V_0/f_0 L_d$) of the outflow. The boundary conditions for $\partial_x \psi$ are then

$$\partial_x \psi = \begin{cases} Ro \, X(x) \, H(t), & y = 0 \\ 0, & y = L, \end{cases} \tag{3}$$

where

$$X(x) = \begin{cases} 1, & |x| < w/2 \\ 0, & |x| > w/2 \end{cases} \tag{4}$$
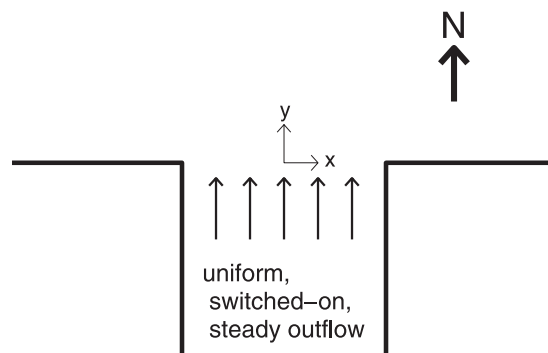


FIG. 1. Poleward outflow in a Northern Hemisphere setting.

and $H(t)$ is the unit step function.

A determination of the proper boundary conditions for $\psi$ involves some subtle details that are presented in the appendix. For mathematical simplicity, we use the boundary conditions

$$\psi = Ro \, \mathcal{X}(x) \, H(t) \quad \text{at} \quad y = 0, \tag{5}$$

$$\psi = 0 \quad \text{at} \quad y = L, \tag{6}$$

where

$$\mathcal{X}(x) = \int_{-\infty}^{x} d\xi \, X(\xi) = \begin{cases} 0, & x < -w/2 \\ x + w/2, & -w/2 < x < w/2 \\ w, & w/2 < x. \end{cases} \tag{7}$$

As described in the appendix, these boundary conditions involve imposing an incoming Kelvin wave from $x = \infty$, with amplitude $Ro e^{-L} w$ on $y = L$. When $L \gg 1$, the appropriate condition for our study, this additional radiation condition has a negligible effect on the solution. Due to the steadiness of the forcing for $t > 0$, the "Kelvin waves" associated with the problem might more appropriately be called "Kelvin currents." In this and the next section, however, our concern with direction of radiation leads us to retain the Kelvin wave terminology, with the understanding that the frequency vanishes after the initial Kelvin waves are set up.

## 3. Solutions

A Fourier sine transform in $y$ and a Fourier transform in $x$ are applied to (1), using the conventions

$$\phi_n(x, t) = \frac{2}{L} \int_0^L dy \, \psi \sin l_n y, \quad \psi(x, y, t) = \sum_{n=1}^{\infty} \phi_n \sin l_n y, \tag{8}$$

$$\overline{\phi_n}^x(k, t) = \frac{1}{2\pi} \int_{-\infty}^{\infty} dx \, \phi_n \, e^{-ikx}, \quad \phi_n(x, t) = \int_{-\infty}^{\infty} dk \overline{\phi_n}^x e^{ikx}, \tag{9}$$

where

$$l_n \equiv \frac{n\pi}{L}. \qquad (10)$$

In the following text, the inverse $y$ transform in (8) will be represented as an infinite sum, to distinguish it from a truly finite sum that will be introduced later. In practice, of course, we truncate the summation at a suitably large value of $n$.

The summation in (8) is not uniformly convergent along the part of the boundary where $\psi \neq 0$, so in applying the transform to the $\partial_{yy}$ term in (1) we integrate by parts, converting the boundary condition at $y = 0$ to a forcing term. Taking the time derivative of the boundary term converts the step function in (5) to a delta function, and the transformed equation becomes

$$\partial_t \overline{\phi_n}^x + i\sigma_n \overline{\phi_n}^x = \frac{2}{L}\text{Ro}\frac{l_n}{k^2 + l_n^2 + 1}\overline{\mathcal{X}}^x \delta(t), \qquad (11)$$

where

$$\sigma_n(k) = \frac{-\beta k}{k^2 + l_n^2 + 1} \qquad (12)$$

and

$$\overline{\mathcal{X}}^x = \frac{\sin(k\,w/2)}{\pi i\,k^2}. \qquad (13)$$

The right-hand side of (11) is nonzero only at $t = 0$, so the solution is just the homogeneous solution. Integrating (11) from $t = -\tau$ to $t = +\tau$, taking the limit as $\tau \to 0$ and considering the quiescent initial condition, yields the value of the multiplicative constant. The solution to (11) for $t \geq 0$ is then

$$\overline{\phi_n}^x = \frac{2}{L}\text{Ro}\frac{l_n}{l_n^2 + 1}\left[\overline{\mathcal{X}}^x - \frac{1}{\pi i}\frac{\sin(k\,w/2)}{k^2 + l_n^2 + 1}\right]e^{-i\sigma_n t}. \qquad (14)$$

## a. The t = 0 solution

A Taylor series expansion of the exponential in (14) shows that there will be an instantaneous, nonzero solution at $t = 0$. For clarity, we separate it into two parts:

$$\overline{\phi_{Kn}}^x \equiv \frac{2}{L}\text{Ro}\frac{l_n}{l_n^2 + 1}\overline{\mathcal{X}}^x \qquad (15)$$

and

$$\overline{\phi_{gn}}^x \equiv -\frac{1}{\pi i}\frac{2}{L}\text{Ro}\frac{l_n}{l_n^2 + 1}\frac{\sin(k\,w/2)}{k^2 + l_n^2 + 1}. \qquad (16)$$

The $x$ transform in (15) is easily inverted, and the terms preceding $\overline{\mathcal{X}}^x$ comprise the Fourier sine transform of the meridional structure of the Kelvin waves, so

$$\psi_K \equiv \sum_{n=1}^{\infty} \phi_{Kn}\,\sin l_n y = \text{Ro}\ \mathcal{X}(x)\ (e^{-y} - e^{-L}e^{y-L}). \qquad (17)$$

Here $\psi_K$ represents the superposition of a Kelvin wave of amplitude $w\text{Ro}$, generated at the outflow and extending eastward along $y = 0$, and the artificially imposed Kelvin wave of amplitude $e^{-L}w\text{Ro}$ incoming from $x = \infty$. Since the Kelvin waves have infinite propagation speeds in the QG framework, they appear fully formed as soon as the outflow is switched on, and it is clear that they will satisfy the boundary conditions for all time. The inverse transform of (16) and higher-order terms in the expansion of the exponential in (14) can only contribute to the interior solution.

By comparison with the $f$-plane solution (not shown) we identify $\overline{\phi_{gn}}^x$ as the transform of evanescent inertia–gravity waves trapped near the corners of the channel mouth. The $x$ transform can be inverted using the residue theorem, giving

$$\phi_{gn} = \frac{1}{L}\text{Ro}\frac{l_n}{(l_n^2 + 1)^{3/2}}\begin{cases} e^{m_n(x+w/2)} - e^{m_n(x-w/2)}, & x < -w/2 \\ e^{-m_n(x+w/2)} - e^{m_n(x-w/2)}, & -w/2 < x < w/2 \\ e^{-m_n(x+w/2)} - e^{-m_n(x-w/2)}, & w/2 < x, \end{cases} \qquad (18)$$

where

$$m_n \equiv \sqrt{l_n^2 + 1}. \qquad (19)$$

The total streamfunction at $t = 0$ is

$$\psi(x, y, t = 0) = \psi_K(x, y) + \psi_g(x, y), \qquad (20)$$

where

$$\psi_g \equiv \sum_{n=1}^{\infty} \phi_{gn}\sin l_n y. \qquad (21)$$

The function $\psi_g$ has a dipole structure that is antisymmetric in $x$, with a peak (trough) trapped near the western (eastern) corner of the outflow channel mouth, and it is an essential part of the solution for an $f$-plane Kelvin wave exiting a narrow channel mouth and rounding the corner. Figure 2 shows $\psi_K$, $\psi_g$, and $\psi(t = 0)$ for two different outflow channel widths. Positive values of the streamfunction are represented by black contours and negative values by gray contours. As expected, $\psi_g$ decays in both $x$ and $y$ and does not contribute to the boundary value of $\psi$. It "smooths" $\psi_K$ so that, once the flow exits the channel mouth, it quickly assumes the characteristic shape of a Kelvin wave rounding a corner, regardless of the channel width. Within a fraction of a deformation radius poleward of the channel mouth, where the streamlines are predominantly oriented north–south, the cross-current Kelvin wave structure is already evident. The meridional velocity at this latitude decays to the west on a deformation radius scale, even though the outflow velocity is uniform across the channel mouth.

On quasigeostrophic time scales, the combined Kelvin–evanescent gravity wave structure appears instantly and can be thought of as the initial condition for the problem. At $x \gg w$ this structure is in geostrophic balance and satisfies the governing equation by itself. In the vicinity of the channel mouth, however, it has a nonzero $\psi_x$ (i.e., meridional velocity) and cannot satisfy (1) without generating time-dependent motions by shedding Rossby waves.

### b. The $t > 0$ solution

When $t > 0$ the solution for the $y$ transform is

$$\phi_n(x, t) = \text{Ro}\, \frac{2}{L} \int_{-\infty}^{\infty} dk \left[ \frac{l_n \sin(k\,w/2)}{i\pi k^2(k^2 + l_n^2 + 1)} \right] \exp\left[ ik\left( x + \frac{\beta t}{k^2 + l_n^2 + 1} \right) \right] \tag{22}$$

The integral cannot be evaluated using the residue theorem because of an essential singularity in the exponential term. The method of stationary phase is typically used to estimate such integrals, but the left-hand term in square brackets is not slowly varying in the vicinity of the important stationary point $k = 0$, that is, near the long Rossby wave front. We therefore solve for the $x$ derivative of the streamfunction:

$$\partial_x \psi = \sum_{n=1}^{\infty} \partial_x \phi_n \sin l_n y, \tag{23}$$

where

$$\partial_x \phi_n = \text{Ro}\, \frac{2}{L} \int_{-\infty}^{\infty} dk \left[ \frac{l_n \sin(k\,w/2)}{\pi k\,(k^2 + l_n^2 + 1)} \right] \exp\left[ ik\left( x + \frac{\beta t}{k^2 + l_n^2 + 1} \right) \right]. \tag{24}$$

The $x$ derivative of $\psi$ is then integrated zonally from a point to the west of the fastest Rossby wave front, where $\psi = 0$.

The stationary phase approximation to (24) is

$$\partial_x \phi_n = Ro\, \frac{4}{L} \frac{l_n}{\pi} \sum_{k_s < 0} \left[ \frac{\sin(k_s\,w/2)}{k_s\,(k_s^2 + l_n^2 + 1)} \right] \sqrt{\frac{2\pi}{t|\partial_{kk}\sigma_n(k_s)|}} \cos\left\{ k_s x - \sigma_n(k_s)t - \frac{\pi}{4} \text{sgn}\, \partial_{kk}\sigma_n(k_s) \right\}. \tag{25}$$

The stationary wavenumbers $k_s$ are found by inverting

$$\frac{x}{t} = \partial_k \sigma(k_s) = \frac{\beta [k_s^2 - (l_n^2 + 1)]}{(k_s^2 + l_n^2 + 1)^2}. \tag{26}$$

In the final solution, $t$ is always found as part of the product

$$\beta t = \beta_0 L_d\, t^* = 2\sigma_{c0}\, t^*, \tag{27}$$
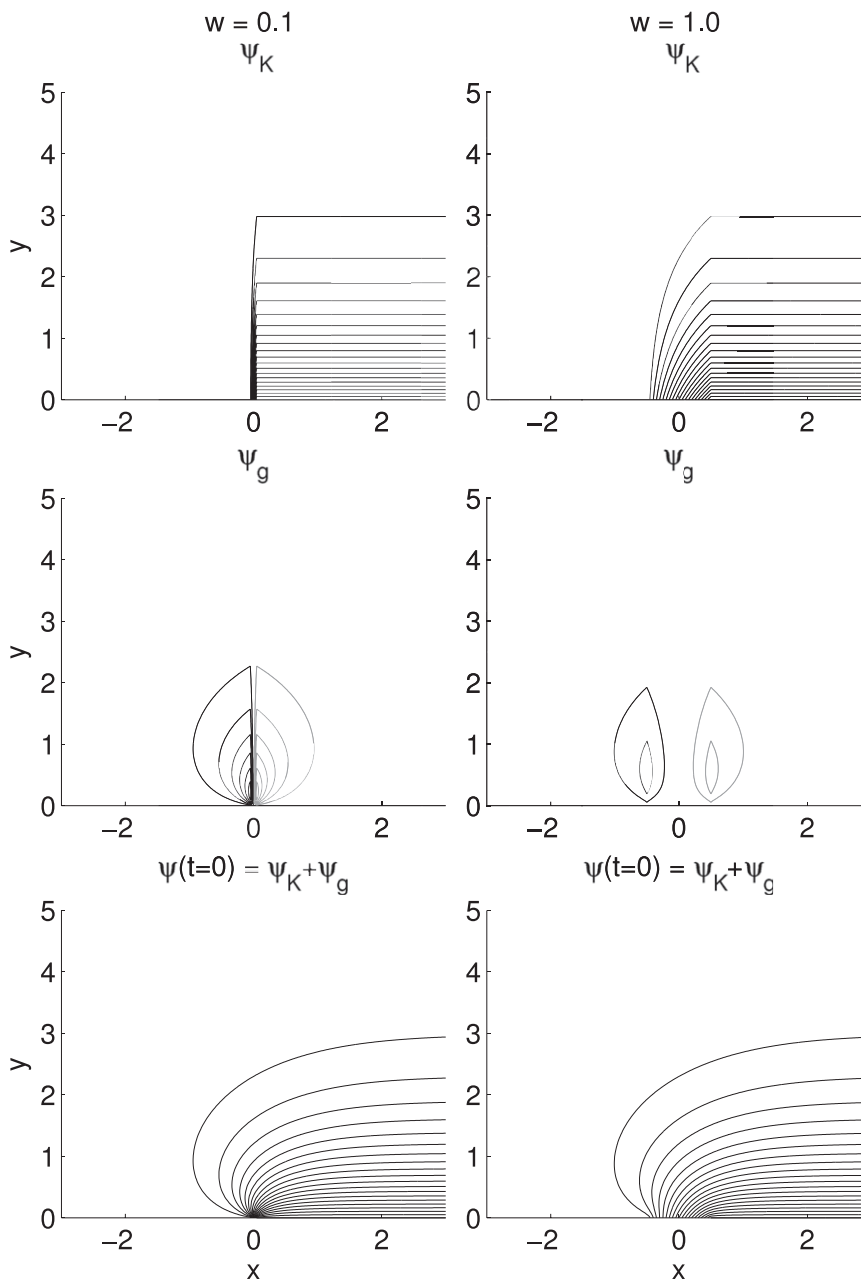
FIG. 2. Solution to the linear quasigeostrophic model at $t = 0$, contours of $\psi/w\text{Ro}$. Black contours: $\psi > 0$; gray contours: $\psi < 0$. (left column) Solutions for $w = 0.1$; (right column) solutions for $w = 1.0$; (bottom row) total streamfunction ($\psi_K + \psi_g$) at $t = 0$.

where $\sigma_{c0}$ is the cutoff frequency for the $l = 0$ Rossby wave at the reference latitude. At the latitude of Lombok Strait, 1 yr is roughly equivalent to $\beta t = 85.5$ for the first baroclinic mode. In the left column of Fig. 3, the stationary phase approximation to the total streamfunction is shown at three successive values of $\beta t$, up to a maximum of 85.5.

In the series of snapshots we see a plumelike feature emanating from the western edge of the Kelvin wave

structure where the nonzero $\beta\partial_x\psi$ term can only be balanced by time dependence. We refer to this feature as the $\beta$ plume and we see that the western front of the plume propagates westward at roughly the long Rossby wave speed. To lowest order there is no mass transport ($\Delta\psi = 0$ across the plume), although there is a westward propagation of streamfunction anomaly. Moving from west to east within a single snapshot, we see that the plume becomes narrower, the peak value of the
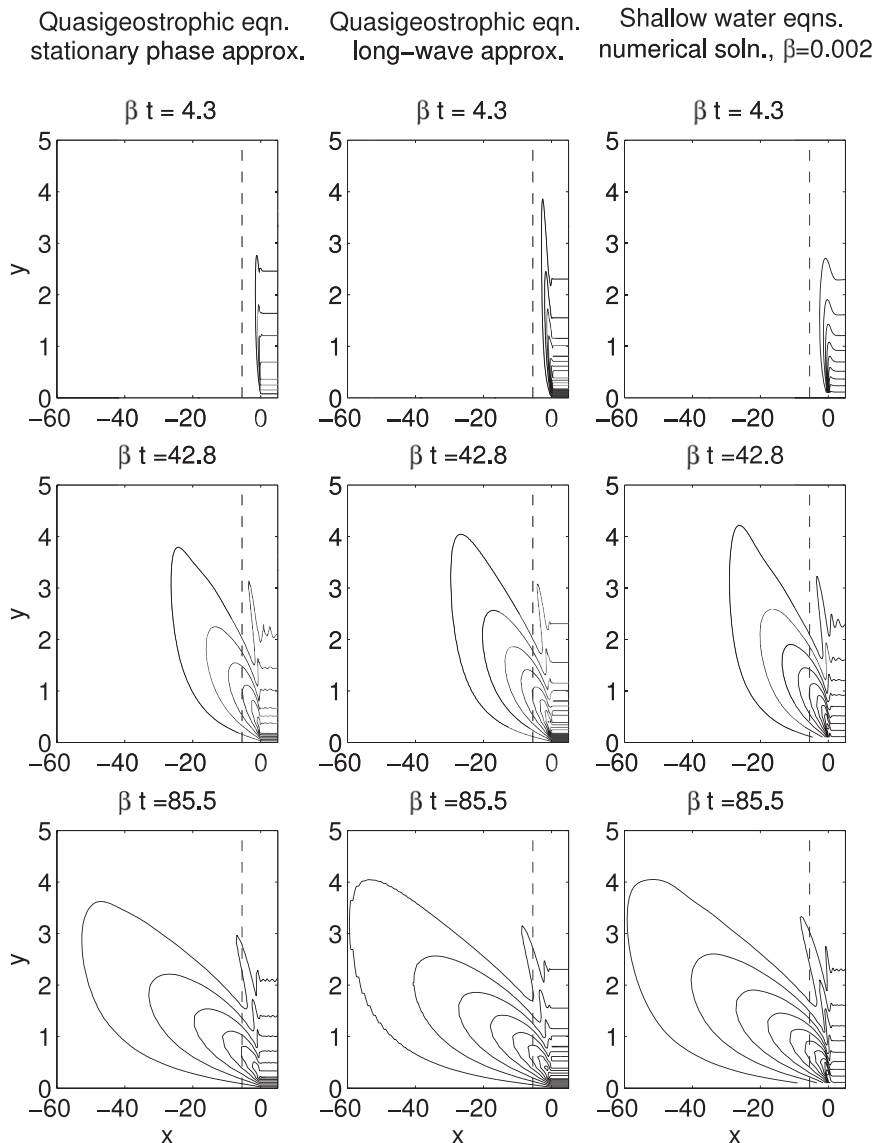
FIG. 3. Comparison of $\beta$-plume propagation in three approximations: (left column) contours of quasigeostrophic streamfunction, stationary-phase approximation; (middle column) contours of quasigeostrophic streamfunction, long-wave approximation; (right column) contours of shallow-water equations' layer-thickness deviation, numerical solution for $\beta = 0.002$ ($\theta_0 = -59.4°$). Dashed lines locate transects at $x = -5.5$.

streamfunction within the plume gets larger, and the locus of the streamfunction peak gets closer to the boundary. Comparing the second and third rows, we see that this progression also holds at a single meridional transect as time passes. Subsequent sections will clarify and quantify these observations.

### c. The long-wave approximation to the quasigeostrophic solution

It is evident from inspection of the left column of Fig. 3 that aside from the immediate vicinities of the channel mouth and the western front, $\partial_{xx} \ll \partial_{yy}$ within the $\beta$ plume (note that in Fig. 3 the $y$ axes are stretched considerably relative to the $x$ axes). Ignoring $\partial_{xx}\psi$ relative to $\partial_{yy}\psi$ simplifies (1) to

$$(\partial_{yy} - 1)\partial_t\psi + \beta\,\partial_x\psi = 0. \qquad (28)$$

With the boundary conditions (5)–(6) and the quiescent initial condition, the transformed solution to (28) is

$$\overline{\phi_{Ln}}^x = \frac{2}{L}\mathrm{Ro}\,\frac{l_n}{l_n^2 + 1}\overline{\mathcal{X}}^x e^{-i\sigma_{Ln}t}, \qquad (29)$$

where

$$\sigma_{Ln} = \frac{-\beta k}{l_n^2 + 1}, \qquad (30)$$

that is, the long-wave ($k \to 0$) limit of the Rossby wave dispersion relation.

The exponential in (29) no longer contains an essential singularity in $k$, and the $x$-transform inversion is straightforward:

$$\phi_{Ln} = \frac{2}{L} \mathrm{Ro} \frac{l_n}{l_n^2 + 1} \mathcal{X}\left(x + \frac{\beta t}{l_n^2 + 1}\right). \qquad (31)$$

The terms preceding $\mathcal{X}[x + \beta t/(l_n^2 + 1)]$ comprise the Fourier sine transform of the Kelvin wave meridional (cross-shore) structure, and each spectral component can be viewed as the amplitude of a distinct meridional mode. For each meridional mode, the $x$ structure of the $y = 0$ boundary condition, $\mathcal{X}(x)$, propagates westward nondispersively at the long Rossby wave speed associated with the appropriate meridional wavenumber, $l_n$. There is a discrete distance between distinct meridional-mode wave fronts and a discrete change in the $y$ structure of the plume with the passage of each wave front. The tapered part of $\mathcal{X}$, corresponding to the channel mouth, merely serves to smooth the transitions. As $L \to \infty$, the discrete spatial and spectral jumps become smaller and smaller so that the tapered part of $\mathcal{X}$ becomes less and less important. We therefore make the further simplification of imagining a delta-function outflow with the same volume flux as would exit a channel of width $w$, thus eliminating the channel mouth taper. The outflow boundary-value structure is then

$$\mathcal{X}_L(x) = w \, H(x). \qquad (32)$$

The solution for this boundary structure, which we will call the "long-wave approximation," is

$$\psi_L(x, y, t) = \mathrm{Ro} \, w \frac{2}{L} \sum_{n=1}^{N(\beta t/x)} \frac{l_n}{l_n^2 + 1} \sin l_n y, \qquad (33)$$

where

$$\frac{L}{\pi} \sqrt{-\left(\frac{\beta t}{x} + 1\right)} - 1 \le N < \frac{L}{\pi} \sqrt{-\left(\frac{\beta t}{x} + 1\right)}. \qquad (34)$$

The summation limit, $N(\beta t/x)$, reflects the fact that only a finite number of meridional modes can reach a given longitude, $x$, within a finite time, $t$. The slower modes do not contribute to the solution at this $x$ and $t$. [Note that the long-wave approximation does not contain the short Rossby waves, so it is appropriate only for $-\beta t \, (L/\pi)^2 < x < 0$.]

The middle column of Fig. 3 shows a time series of snapshots of the $\psi_L$ plume taken at the same times as those in the left column (stationary-phase approximation to the complete QG problem). The westward propagation is somewhat faster in the long-wave approximation, which we expect because the approximation overestimates the group velocity of each meridional mode. Otherwise, the match is very good.

### d. Plume evolution

The long-wave approximation presents an easy way to conceptualize and to quantify the temporal and spatial changes in the plume structure that we noticed in the stationary-phase solutions. We think of the individual Fourier components of the Kelvin current's cross-shore structure as representing the amplitudes of individual meridional Rossby modes. The Rossby adjustment of the $t = 0$ Kelvin current's western front (where outflow streamlines cross planetary vorticity contours) consists of the Rossby modes propagating westward with group velocities that decrease as the meridional mode number increases. The spectrum of the plume's meridional structure at a given longitude is just a truncated version of the Kelvin current's spectrum, and the truncation limit increases monotonically as time passes and additional Rossby modes are able to reach that longitude.

When $N = 1$, the plume has the $y$ structure of the half-sine wave on the channel width. The passage of the next mode, $N = 2$, enhances the half of the plume closest to $y = 0$ and detracts from the other half. As time proceeds, the peak of the plume continues to increase in amplitude and shift toward $y = 0$ while the width of the plume decreases. As $N \to \infty$, the plume approaches the meridional structure of the preexisting eastward Kelvin current with a delta-function westward current along the boundary. As mentioned previously, the summation in (8) is not uniformly convergent for $x > -w/2$, so in that part of the domain the delta-function feature is just a mathematical artifact of the sine transform representation of $\exp(-y)$. For $x < -w/2$, however, the series is uniformly convergent, and the delta-function feature is an essential part of the inviscid dynamics. As $t \to \infty$, the steady state that emerges consists of the flow exiting the channel and turning westward toward $x = -\infty$ in a delta-function boundary current. Superimposed on this narrow westward boundary current of semi-infinite length is an eastward Kelvin current with equal and opposite volume transport, extending from $x = -\infty$ to $x = \infty$.

We are not so much interested in the $t \to \infty$ structure as we are in the plume evolution at shorter times, and we are particularly interested in how well the simple long-wave expression (33) predicts this evolution. Figure 4 shows the $y$ structure of the plume measured at
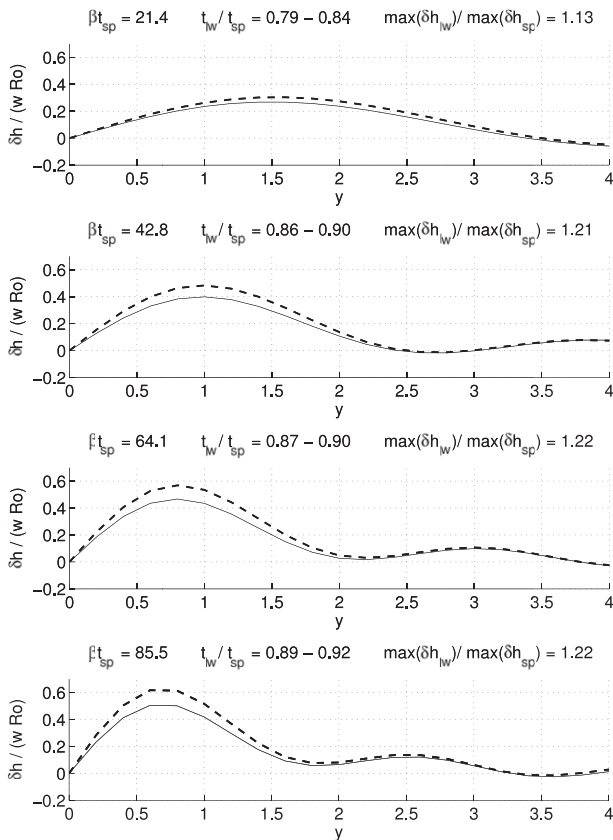
FIG. 4. Beta-plume evolution at $x = -5.5$. Solid lines: stationary phase (sp) approximation. Dashed lines: long-wave (lw) approximation. Ratio of times, $t_{lw}/t_{sp}$, each approximation takes to evolve to displayed profile.

four successively longer times at the transect $x = -5.5$ (shown in Fig. 3 panels as a dashed line). The solid lines represent the stationary-phase approximation at the given values of $\beta t$, and the dashed lines represent the long-wave approximation, with $N$ chosen in each case to give the best match with the plume width and peak location in the stationary-phase approximation. Using (34) the $t$ required for the long-wave approximation to achieve the displayed profile is calculated, and the ratio of the long-wave approximation $t$ to the stationary-phase approximation $t$ is presented in each panel. Because of the discrete nature of the long-wave approximation evolution, this ratio is given as a range, the width of which depends on the channel width used in (33)–(34). The qualitative match between the stationary-phase approximation and the long-wave approximation is quite good, although the long-wave approximation plume evolves about 11% faster and has a peak amplitude about 23% greater for the same plume width. The evolutionary process described above is clearly representative of the full quasigrostrophic solution—it is just easier to visualize

in the long-wave approximation owing to the nondispersive nature of the individual meridional modes and the simplicity of (33).

Both the stationary-phase and long-wave solutions are approximations, and it is not immediately obvious which of the traces in Fig. 4 is more representative of the true solution. We therefore compare these solutions with numerical solutions (another approximation) of the linearized SWE on the $\beta$ plane. The equations and numerical model are described in DSP, and at midlatitudes and long time scales we expect a good match between the SWE and QG solutions.

The right column of Fig. 3 shows snapshots of the $\beta = 0.002$ numerical plume ($\theta_0 = 59°$), taken at the same times as the QG solutions in the other columns. The contours are of the layer thickness deviation, and the agreement with the streamfunction contours of the QG solutions is quite good. As expected, the numerical plume evolution near the channel mouth is slower than that of the long-wave approximation, but the qualitative match between the numerical and long-wave plumes appears better than the match between the numerical and stationary-phase plumes.

Figure 5 is the equivalent of Fig. 4, with the numerical plume evolution at $x = -5.5$ represented by the solid lines, and the long-wave approximation represented by the dashed lines. The long-wave approximation evolves roughly 10% faster, but the general agreement is better than between the long-wave and stationary-phase solutions (Fig. 4). Note that we are referring to the evolution at $x = -5.5$ (dashed lines in Fig. 3). The western front of the plume appears to evolve at the same rate in both the numerical and long-wave solutions (bottom row, Fig. 3).

The long-wave approximation underestimates the numerical plume's peak by only a few percent, whereas it overestimates the stationary-phase solution by about 10%. The stationary-phase approximation involves a truncation of the transform-inversion integral, and the approximation technically requires $t \to \infty$. We should not be surprised then that, while it provides an excellent qualitative approximation of the solution, the stationary-phase approximation appears to provide a quantitative underestimate at the finite times that we are considering.

In DSP we seek to understand numerical solutions to the SWE. Given the good agreement in Figs. 3 and 5 between the numerical SWE solutions and the long-wave solutions to the QG equation, we feel confident that the long-wave approximation captures the essence of the linear SWE plume development at midlatitudes.

This section has presented the plume evolution as a function of time at a fixed $x$, but (34) shows that the same pattern can be viewed as a function of $x$ at a fixed time.
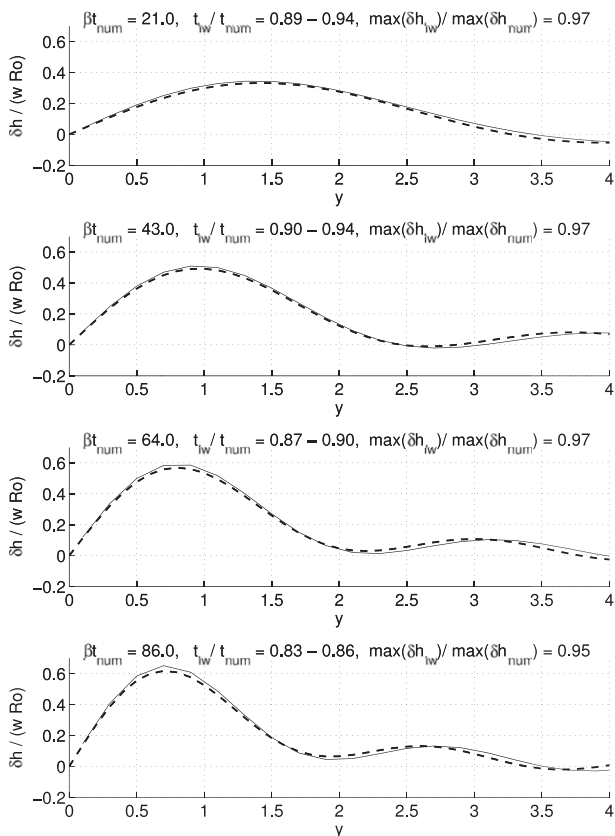
FIG. 5. Beta-plume evolution at $x = -5.5$. Solid lines: numerical (num) solutions of the linear shallow-water-equation thickness deviation ($\delta h$) with $\beta = 0.005$. Dashed lines: long-wave (lw) approximation of the linear QG streamfunction ($\psi$). Ratio of the times, $t_{lw}/t_{num}$, that the two approximations take to evolve to the displayed profiles.

Viewing a snapshot of the plume (e.g., bottom row, Fig. 3), the change in cross-shore structure as we move from west to east is identical to the evolution with time at a given longitude. As long as $t < \infty$ the plume continues to evolve and is never truly zonal. In DSP we will see that this situation changes when nonlinearity is introduced.

## 4. Summary

On QG time scales, the response to a switched-on, steady poleward outflow is the instantaneous setup of a Kelvin current carrying 100% of the outflow to the east of the channel mouth. At $t = 0$, the western front of the current is not in geostrophic balance and it adjusts by shedding Rossby waves in a process that is easily conceptualized. Each of the Fourier-transform components of the Kelvin current's offshore structure propagates westward with its own distinct group velocity. As the individual wave fronts pass a given meridional transect, the plume cross-section changes. It starts with a low-

amplitude peak far offshore and evolves monotonically with the streamfunction peak becoming larger and migrating toward shore. The "long-wave approximation," in which the individual Rossby waves are considered nondispersive, provides a good estimate of the plume's meridional structure and amplitude. Although it overestimates the evolutionary rate by some 10%, it provides an easy way to predict the nature of the plume's evolution using (33) and (34).

As noted, 100% of the outflow volume flux is carried westward by the Kelvin current. Any volume flux associated with the westward propagation of streamfunction anomaly is a second-order effect in the QG formulation. The Kelvin current also carries 100% of the outflow energy flux. This can be seen either by integrating $\partial_y \psi^2$ across the plume or by considering the ratio of Rossby wave group velocity to Kelvin wave group velocity, a ratio which vanishes in the QG approximation.

## APPENDIX

### Boundary Conditions for the Quasigeostrophic Streamfunction

Prior to $t = 0$, the quasigeostrophic streamfunction is zero along $y = 0$. When $t > 0$ the streamfunction has a constant value along ($x < -w/2$, $y = 0$) and a different constant value along ($x > w/2$, $y = 0$). In addition to Rossby waves, the QG model can represent coastal Kelvin waves with constant phase along a zonal boundary (i.e., infinite phase speed). These correspond to the $\partial_x \psi = 0$, $(\partial_{yy} - 1)\psi = 0$ solution of the vorticity equation (1). Because the Rossby waves have finite group velocities, only the Kelvin waves can instantly set up the $\Delta \psi$ across the channel mouth at $y = 0$ while maintaining constant streamfunction values on ($x < -w/2$, $y = 0$) and ($x > w/2$, $y = 0$). With the temporal step function forcing, the Kelvin wave phase will also remain constant in time after being switched on (i.e., the zero-frequency limit), thus maintaining the boundary conditions for all time. Consequently, the Rossby waves do not contribute to the boundary values of the streamfunction at any time.

In a channel of width $L$ the outflow can produce both an eastward Kelvin wave with streamfunction value $\psi_e$ on $(x > w/2, y = 0)$ and a westward Kelvin wave with streamfunction value $\psi_w$ on $(x < -w/2, y = L)$. The eastward Kelvin wave only contributes to streamfunction boundary values east of the channel mouth, and the westward Kelvin wave only contributes to boundary values west of the mouth. When $t > 0$ the natural radiation condition of no incoming signal from $x = \infty$ leads to a streamfunction value on $y = L$ east of the channel mouth equal to $\psi_e \, e^{-L}$, due to the eastward Kelvin wave trapped at the $y = 0$ boundary. Likewise, no incoming signal from $x = -\infty$ gives a streamfunction value on $y = L$ west of the mouth equal to $\psi_w$. The $y = L$ streamfunction values east and west of the mouth must be equal to prevent flow through the poleward boundary:

$$\psi_w = \psi_e \, e^{-L}. \tag{A1}$$

Likewise, the boundary value on $y = 0$ west of the channel mouth is $\psi_w \, e^{-L}$, due to the westward Kelvin wave trapped at $y = L$. Using (A1) we see that this value is equal to $\psi_e \, e^{-2L}$, and the change in streamfunction value across the channel mouth at $y = 0$ is

$$\Delta\psi \equiv \psi(x = w/2, y = 0, t > 0) - \psi(x = -w/2, y = 0, t > 0)$$
$$= (1 - e^{-2L}) \, \psi_e. \tag{A2}$$

Integrating the velocity boundary condition (3) across the channel mouth, we also have

$$\Delta\psi = \text{Ro} \, w, \tag{A3}$$

and we find that

$$\psi_e = \frac{\text{Ro} \, w}{(1 - e^{-2L})}. \tag{A4}$$

The proper boundary conditions for the streamfunction when $t > 0$ are then

$$\psi(x < w/2, y = 0) = \frac{e^{-2L}}{1 - e^{-2L}} \, \text{Ro} \, w, \tag{A5}$$

$$\psi(|x| < w/2, y = 0) = \frac{e^{-2L}}{1 - e^{-2L}} \, \text{Ro} \, w + \text{Ro} \, (x + w/2), \tag{A6}$$

$$\psi(x > w/2, y = 0) = \frac{1}{1 - e^{-2L}} \, \text{Ro} \, w, \tag{A7}$$

$$\psi(x, y = L) = \frac{e^{-L}}{1 - e^{-2L}} \, \text{Ro} \, w. \tag{A8}$$

These boundary conditions are mathematically cumbersome, and we prefer to fix the streamfunction values for $(y = L)$ and $(x < -w/2, y = 0)$ at their initial values for all time. This amounts to imposing a radiation condition that includes a Kelvin wave incoming from $x = \infty$, which is trapped at the $y = L$ boundary and has an amplitude there of

$$\left( \frac{-e^{-L}}{1 - e^{-2L}} \right) \text{Ro} \, w.$$

This incoming wave subtracts from the streamfunction boundary values at all $x$ and cancels the westward Kelvin wave induced by the outflow. With the added radiation condition, the boundary conditions for $t > 0$ are (5)–(6), reproduced here:

$$\psi = \text{Ro} \, \mathcal{X}(x) \, H(t) \quad \text{at } y = 0,$$

$$\psi = 0 \quad \text{at } y = L,$$

with $\chi(x)$ as in (7). While the above radiation condition seems artificial, it greatly simplifies the mathematics, and for a channel width greater than a few deformation radii ($L \gg 1$), the effect on the solution is negligible. The simpler boundary conditions have the added benefit that we can use a Fourier sine transform in $y$ on the governing equation and the inverse transform will be uniformly convergent on $x < w/2$, where the most interesting part of the solution will be found.

### REFERENCES

Durland, T. S., M. A. Spall, and J. Pedlosky, 2009: Response to a steady poleward outflow. Part II: Oscillations and eddies. *J. Phys. Oceanogr.,* **39,** 1551–1573.

Feng, M., and S. Wijffels, 2002: Intraseasonal variability in the South Equatorial Current of the east Indian Ocean. *J. Phys. Oceanogr.,* **32,** 265–277.

Nof, D., T. Pichevin, and J. Sprintall, 2002: "Teddies" and the origin of the Leeuwin Current. *J. Phys. Oceanogr.,* **32,** 2571–2588.

Pedlosky, J., 1987: *Geophysical Fluid Dynamics.* 2nd ed. Springer-Verlag, 710 pp.

Yu, Z., and J. Potemra, 2006: Generation mechanism for the intraseasonal variability in the Indo-Australian basin. *J. Geophys. Res.,* **111,** C01013, doi:10.1029/2005JC003023.